1 October 1999

ELSEVIER

Optics Communications 169 (1999) 141–148

OPTICS COMMUNICATIONS

www.elsevier.com/locate/optcom

Development of a 25 W TEM_{00} diode-pumped Nd:YLF laser

M. Armstrong [a], X. Zhu [b], S. Gracewski [c], R.J.D. Miller [d,*]

[a] *Department of Physics and Astronomy, University of Rochester, Rochester, NY 14627, USA*
[b] *NRC / Integrated Manufacturing Technologies Institute, Room 2077, 100 Sussex Drive, Ottawa, ON, Canada*
[c] *Department of Mechanical Engineering, University of Rochester, Rochester, NY 14627, USA*
[d] *Departments of Physics and Chemistry, University of Toronto, 60 St. George Ste., Toronto, ON, Canada M5S 1A7*

Received 18 March 1999; received in revised form 9 July 1999; accepted 21 July 1999

Abstract

We report the design and the operation of a novel two-head, side-pumped Nd:YLF laser that generates up to 25 W TEM_{00} output power at 1.053 μm. The anisotropic thermal lensing of each laser head has been examined and compensated with cylindrical lenses. The output power of this two-head laser exhibits excellent dynamic range with a typical optical–optical conversion efficiency of 18%. © 1999 Elsevier Science B.V. All rights reserved.

Keywords: Diode-pumped laser; High power laser; Thermal lensing; Nd:YLF

1. Introduction

In the past decade, there have been significant strides in the development of high power diode-pumped solid-state lasers (DPSSL). DPSSLs are already available in commercial products employed in a variety of applications [1,2]. Despite this progress, scaling to higher power with good efficiency still remains an obstacle. There have been a number of schemes developed to reduce the magnitude of the thermal lens and associated thermal aberrations. One approach has been to use a slab design to average out the thermal effects along the axis used for cooling the laser gain medium. This approach, with well designed slab parameters, has achieved as much as 100 W outputs in a high quality beam [3,4]. The other approach is to use 1-D cooling along the beam propagation direction and very thin laser discs to keep the rod temperature in a usable range. This thin disc concept has also demonstrated TEM_{00} operation with powers beyond 100 W [5]. These results are significant and illustrate that diode laser pumping can be scaled to higher brightness than that possible with conventional lamp pumped systems. Each of the above approaches has certain advantages and disadvantages in implementation and cannot be applied to all laser materials. In particular, scaling to the 30 W level with 20% efficiency is difficult in materials like Nd:YLF, due to a variety of material parameter limitations: relatively low gain (1.053 μm transition), power thermal fracture limits and low absorptivity at the pump wavelengths. However, Nd:YLF is desir-

* Corresponding author. E-mail: dmiller@lphys.chem.utoronto.ca

PII: S0030-4018(99)00399-5

able in some industrial Q-switching applications for its less severe thermal lensing [6,7], and high energy storage capacity [8]. There is a need for different cavity designs which permit power scaling using standardized diode laser pump modules which is amenable to a wide class of laser materials. In this paper, we report the performance of a diode-pumped Nd:YLF laser in a symmetric two-head configuration which can generate an output power of up to 25 W with an excellent dynamic range.

2. Experimental results

A schematic of the laser cavity design is illustrated in Fig. 1(a). The laser cavity contains two laser heads, each of which consists of an 8.2 cm long, Brewster-cut Nd:YLF rod with a cross section of 3×2 mm^2. The rod is pumped from the side by four 20 W in-line CW diode arrays (Optopower) collimated with 0.8 mm diameter fiber lenses. The pump passes through the crystal and is then back reflected at an angle by metal coated prisms mounted behind the rod as shown in Fig. 1(b) [9]. The rod is mounted in a water flow cell which cools the surface over ~ 77 mm of the length of the rod. We estimate the losses due to coupling optics to be around 10–15% and we assume $\sim 90\%$ of the remaining pump light is absorbed in the rod. To compensate the pump induced thermal wedge, the two heads are pumped from opposite directions. Both the rods and diodes in this laser are water cooled and all results were obtained with a water temperature of 14°C. This relatively cold water temperature is necessary to keep the diodes used in this study tuned to the absorption of Nd:YLF at 797 nm. The laser cavity has a length of 90 cm with two cylindrical lenses located between the rods and the end mirrors as shown in Fig. 1. Each end mirror has a radius of curvature of 2 m and the cavity is point-symmetric about its center. The cavity was operated with two sets of cylindrical lenses. The cylindrical lenses both have a focal length of 75 cm and are located approximately 1.5 cm from the end mirrors. The lenses focus in the vertical direction and compensate the thermally induced astigmatism in each head.

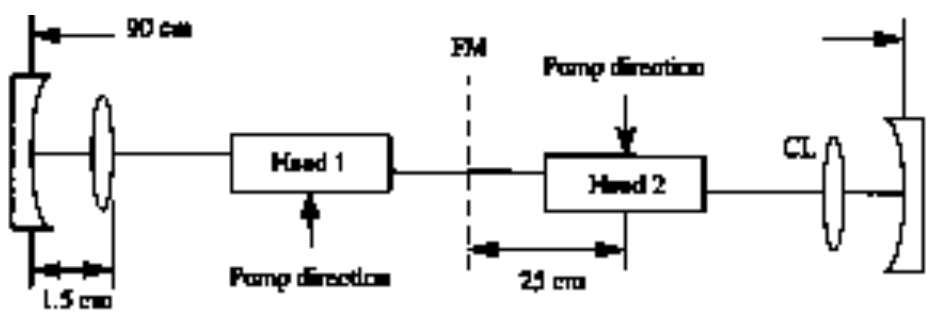

(a) M, 2 m radius end mirror; CL, 75 cm focal length cylindrical lens; FM, flat mirror for turning each head individually.

(b) Pumping scheme.

Fig. 1. Cavity and pumping scheme.

Thermal lensing in Nd:YLF is both astigmatic and polarization dependent [7,10,11]. To minimize the effects of thermal lensing, the rods were Brewster cut appropriate for lasing on the 1.053 μm line in Nd:YLF. For our pumping configuration, the thermal lens was positive in the horizontal direction (along the laser polarization) and negative in the vertical direction. The thermal lens of each head was determined by propagating a horizontally polarized, collimated He–Ne laser beam through the pumped rod and locating a focus in the horizontal direction. The focal length of the induced thermal lens as a function of pump power for both laser heads is shown in Fig. 2. The pump power is derived from the diode manufacturer's measurements of the uncollimated diode output as a function of current. As expected, the focal length is inversely proportional to the pump power. More specifically, a thermal lens of focal length 70–80 cm at 30 W pump changes to approximately 40–45 cm at 60 W pump. We estimate a thermal lensing coefficient k of 2–3 $m^{-1}/[kW/cm^2]$ according to $1/f = k(P/A)$, where f is the focal length, P is the absorbed pump power, and A is the rod cross-sectional area. This result clearly demonstrates that stronger thermal lensing than lamp pumped systems may exist even in side-pumped system (cf. Vanherzeele [7]). Although the total deposited power into the rod in our diode pumped system is less than comparable flashlamp pumped systems, the pump density and associated thermal gradient is actually higher.

After characterizing the thermal lensing properties of both laser heads, we individually tested the laser performance of each head by placing a flat high reflecting mirror in the center of the symmetric cavity as shown in Fig. 1. This allowed us to characterize the single head performance with approximately the same cavity configuration as the dual head configuration. The power output for laser head '2' under these conditions is shown in Fig. 3. The solid curve shows the output power as a function of pump power for the laser optimized near threshold, whereas the dashed curve shows the output for the laser optimized near the maximum pump power. In each case, the laser was optimized at near threshold/maximum pump power and then the pump power was increased/decreased by changing the pump current without any realignment of the cavity. By comparing the two curves one can see an obvious hysteresis in the output power, which we believe was mainly due to an asymmetric pump induced wedge-like phase distortion in the rod. A similar power hysteresis was also observed in laser head 1. However, as a result of better diode collimation, laser

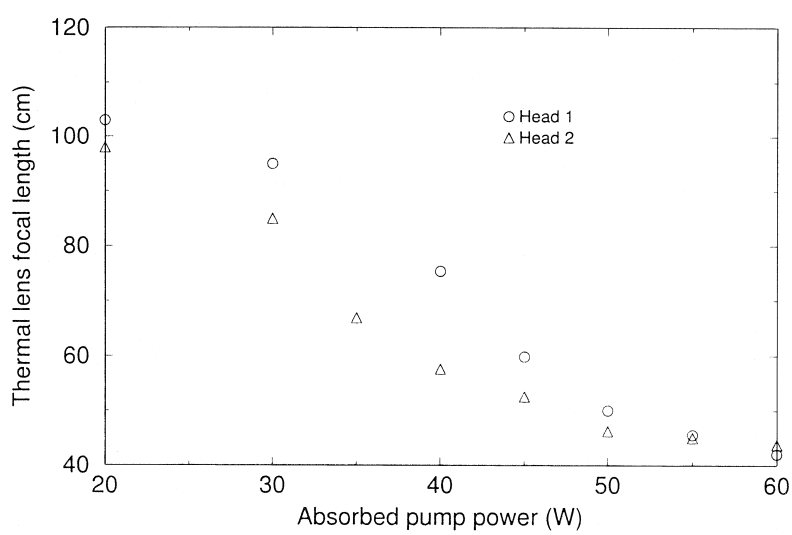

Fig. 2. Focal length of the thermal lens in the horizontal plane for each head as a function of pump power. The lens in the vertical plane has approximately the same magnitude and is opposite in sign.

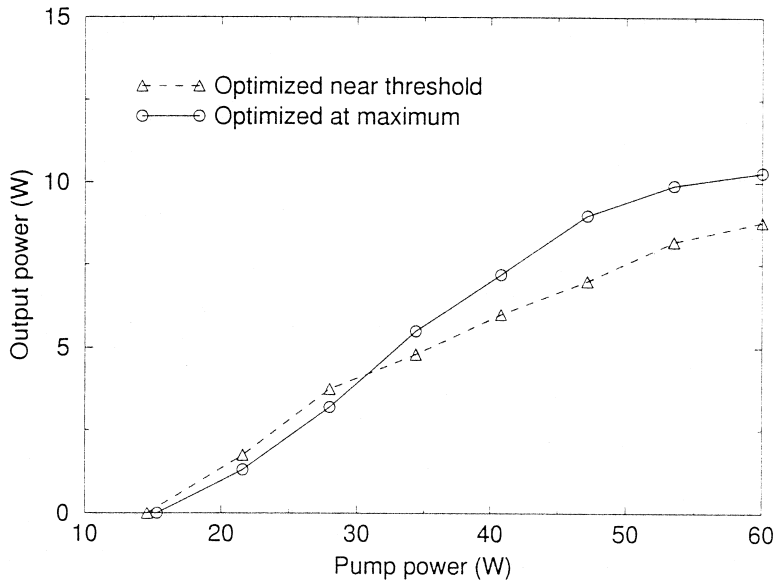

Fig. 3. Laser head 2 output power as a function of pump power.

head 1 generated a maximum of 14 W with the same 20% output coupler used for laser head 2.

The most straightforward way to scale laser power to the 20 W level is to use multiple head designs. The key distinction of this work is the implementation of a symmetric design that cancels the inherent asymmetric thermal aberrations associated with side pumping. The primary objective is to have a system with linear response over the complete power range.

A two-head laser has the advantage of distributing the focusing power of the rods symmetrically in the cavity, so that the overall lensing in the cavity is

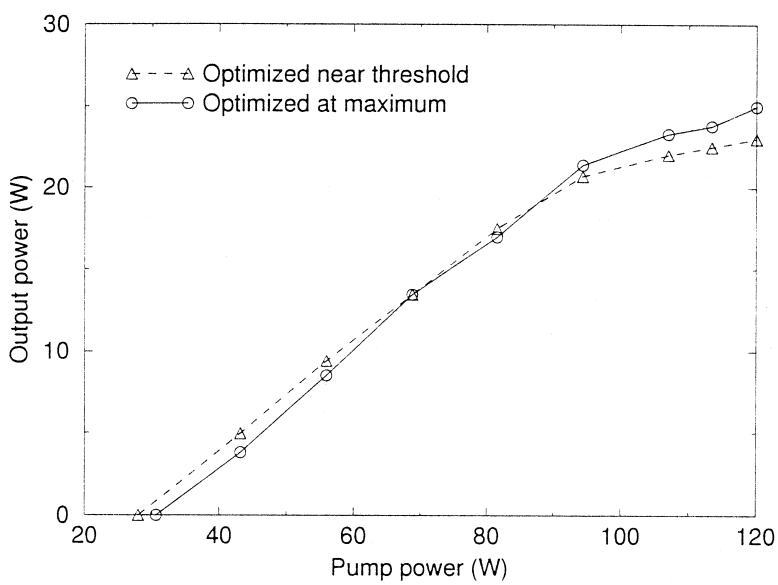

Fig. 4. Output of two-head laser as a function of total pump power.

reduced [12]. In addition, this design allows self-correction of the thermally induced wedge by pumping each rod from the opposite side which can reduce the power hysteresis observed in the single laser head cavities. The measured power hysteresis curve of the two-head system with 30% output coupler is shown in Fig. 4. Between threshold and 20 W output power, the laser output exhibits minimal power hysteresis compared to the single head cavity, shown in Fig. 3. Also, the output power is nearly linear with the pump power up to 20 W, which is an exceptional dynamic range for a laser of this power level. The change in slope efficiency is near the maximum output of the laser diode arrays and does not correspond to the inherent stability range of this approach. At higher diode currents, the diode laser pump broadens and the optical coupling efficiency decreases. The magnitude of the thermal lens is small enough that, with proper cavity design, powers up to the 50 W range should be achievable in a diffraction limited beam with good dynamic range. The maximum optical to optical efficiency, at a pump power of 120 W absorbed pump power, is 18%. To quantify the beam quality, M^2 measurements were conducted using the knife-edge method. An M^2 of 1.2 in both horizontal and vertical directions was measured.

3. Modeling

In the interest of better understanding the origin of the highly anisotropic thermal lens in our rod, we calculated the thermally induced phase distortion over the rod profile. Typically, a complete calculation of the thermal phase distortions in a solid state laser rod must include contributions from three effects (from most to least significant): (1) first order change in bulk index with temperature; (2) deformation of the ends of the rod due to thermal expansion; and (3) stress induced index changes via the elasto-optic effect [13,14]. We did not include a contribution from the elasto-optic effect because this usually accounts for a only small fraction of the total thermal lens ($\sim 5\%$) [13] and, furthermore, the relevant elasto-optic coefficients for YLF were not available at the time of publication. We also did not include deformation in this calculation, since, for a moderate amount of absorption (5 cm^{-1}) with our pumping configuration, less than 1% of the pump light will be absorbed within 5 mm of the end of the rod. Modeling of a number of different pump geometries has shown that significant deformation will occur only for heat deposition near the face of the rod [15].

In contrast to most end-pumped systems, the heat deposition in our system is highly asymmetric. Though both the end-face deformation and elasto-optically induced index changes may be anisotropic in an end-pumped YLF rod, we do not expect a large contribution due to deformation in this system. We believe the anisotropic thermal lens in our system is primarily due to the highly inhomogeneous heat deposition in our rod combined with anisotropic convective cooling.

The calculations were performed using the NASTRAN finite-element analysis program [16] to solve for a temperature distribution in the rod given by the static diffusion equation:

$$\rho = K\nabla^2 T \tag{1}$$

where ρ is the heat density deposition rate, K is the thermal conductivity and T is the temperature.

Due to the asymmetry of the pump intensity distribution, a three dimensional model is required. Assuming a coordinate system with its origin at the center of the rod, the z axis parallel to the optical axis and the x axis along the direction of the pump propagation, the model pump intensity distribution is symmetrical with respect to the x–y and x–z planes. Therefore, it is enough to consider only the positive z, positive y quadrant of the rod. Our model consists of the upper right quadrant of the rod as seen viewing along the pump direction, measuring 40 mm in length, 1.5 mm in height and 2.0 mm in depth. The model is evenly divided with 120, 15 and 20 elements, respectively, along the axes.

The calculated optical path difference (OPD) profile is shown in Fig. 5. It shows the difference between the optical path length (OPL) through the rod at ambient temperature and the OPL under pumping conditions. After using the finite element analysis to determine a temperature distribution in the rod, the total optical path difference is determined by integrating a local change in the optical path length along the optical axis (z axis), i.e. [14],

$$\mathrm{d}OPD(x,y,z) = \frac{\partial n}{\partial T} T(x,y,z)\,\mathrm{d}z \tag{2}$$

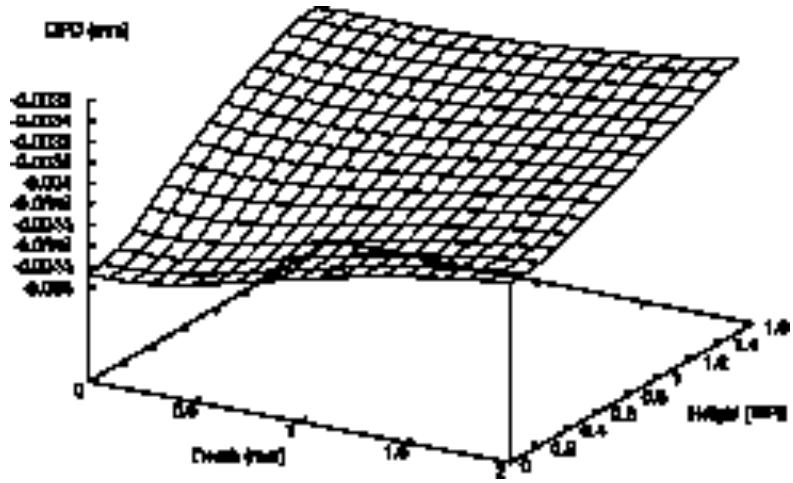

Fig. 5. Calculated optical path difference profile of the top half of our side-pumped rod. The pump beam is centered along the x axis of this graph and travels in the positive x direction.

where we are considering only the contribution from the thermal dispersion, $\partial n/\partial T$. The beam is assumed to be large and well-collimated at the input of the rod.

The local change in index is negative ($\partial n/\partial T = -2\times10^{-6}$ for YLF) for a positive change in the temperature, so the OPD is negative over the entire rod profile. The model assumes conduction cooling with a surface heat transfer coefficient of 1000 W/[m^2 K] on the surface of the rod, corresponding to estimates of the cooling efficiency based on the water flow on these surfaces. Although the maximum temperature in the model depends strongly on the cooling efficiency, the thermal lens is relatively insensitive as a result of convective cooling. The pump distribution was modeled as a 1.0 mm high, 40 mm wide top-hat beam propagating along the x axis and polarized along the extraordinary axis of the crystal (the y axis in our model). We assume 60 W of absorbed pump power per head and that 30% of the absorbed pump energy is deposited as heat.

Cuts of the OPD profile along the x and y axes are shown in Figs. 6 and 7. Least square fits of the OPD curvature along the vertical and horizontal directions (in the center of the rod) over the beam profile (assumed to be 1 mm in diameter) give values of the thermal lens in the vertical and horizontal planes of -51 cm and 1.44 m, respectively. These numbers should be compared with the measured thermal lens focal lengths, which were around 45 cm in magnitude for both the vertical and horizontal with a positive thermal lens in the horizontal and a negative thermal lens in the vertical. Although the OPD profiles deviate from the least square parabolic fits outside the intracavity mode size (about 1 mm in diameter), the profile along the vertical direction in particular is very close to parabolic over the size of the beam (centered on the rod). The calculated OPD fits a parabolic plus wedge fit accurately in the horizontal plane (over the beam profile) for a 1 mm beam centered around 1.2–1.3 mm from the pump side of the rod.

The agreement in both sign and magnitude is very good for the vertical direction, whereas there is a factor of approximately three difference in magnitude between the calculated and measured result along the horizontal axis. We anticipate an error in the calculation may be as high as 50%, due to inaccuracy in the specification of the pump distribution (15%), disregarding the deformation and elastooptic terms (15%), and errors in the estimate of the physical parameters, such as the absorption coefficient and the first order change in index with the temperature (20%). Furthermore, the He–Ne probe beam used to diagnose the thermal lens may not have precisely traced the path of the intracavity laser mode through the rod and this, for the horizontal lens measurement in particular, may explain the discrep-

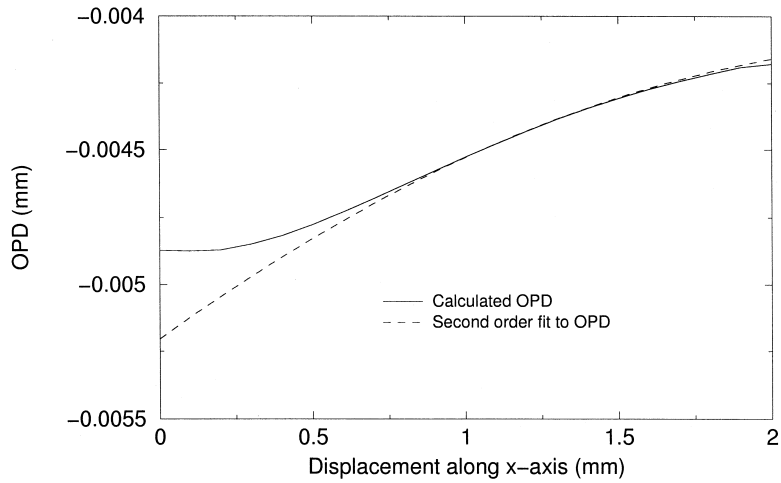

Fig. 6. Calculated optical path difference profile along the x axis and fit.

ancy between the measured and calculated values for the horizontal thermal lens. The essential features of the thermal lensing have been captured in the modeling. Within the accuracy of the various parameters the magnitude of the calculated thermal lens is in qualitative agreement with measurements. This code has been checked against a number of literature reports of thermal lensing in symmetric end-pumped situations and typically gives thermal lens values within 20% of the reported value for Nd:YAG. Based on these results, we attribute the discrepancy between theory and experiment (for the lens along the x axis) in this study to features in the rod flow cell that lead to anisotropic cooling and enhanced

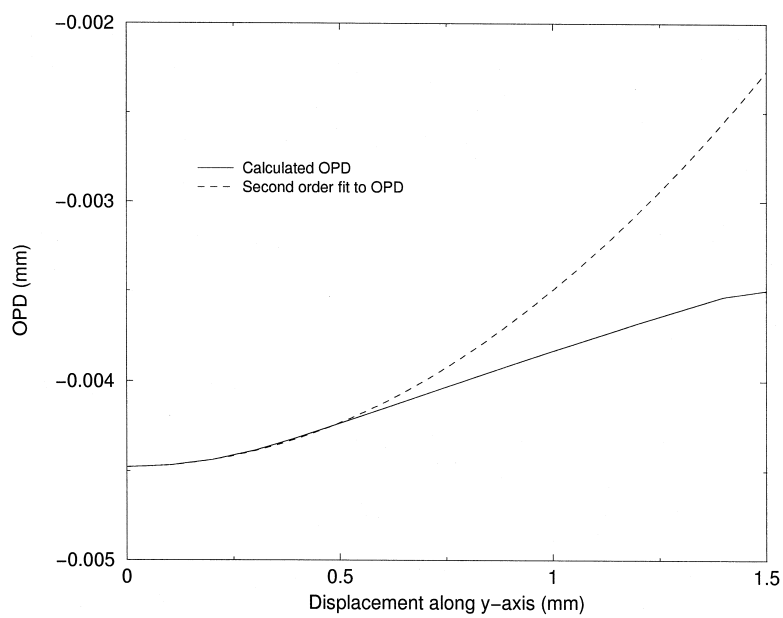

Fig. 7. Calculated optical path difference profile along the y axis and fit.

anisotropy in the thermal lens. For most effective cooling, all four sides of the rod are water cooled. The laser diodes pump through an optical input window. To minimize absorption of the pump radiation and turbulence effects, the path length through the water was made as small as possible on both the input and exit surfaces. The flow and cooling is more efficient along the vertical direction. Strongly anisotropic cooling could significantly increase the anisotropy in the thermal lens.

Despite this limitation, these calculations can be used to determine the potential for further scaling of output power. Given the magnitude of the lens, the symmetrizing feature of the dual head approach (removal of thermal wedge effect) should permit scaling up to the 50 W power level for a YLF system.

4. Summary

To summarize, we have developed a diode-pumped Nd:YLF laser with TEM_{00} output power in the 30 W range with exceptional dynamic range. The laser system has also been successfully Q-switched at repetition rates as high as 20 KHz with only a 10% change in average power from CW operation and no other change in performance. To our knowledge, this is the first diode-pumped Nd:YLF laser to attain this power level at 1.053 μm. The laser system is based on standard components and laser rod assemblies such that implementation is relatively straightforward. The laser cavity is a simple symmetric design which effectively compensates the anisotropic thermal lensing and reduces power hysteresis effects due to the thermally induced wedge in side pumped laser rods. Further improvement in both power and beam quality may be possible by replacing the cylindrical lenses with appropriate cylindrical end mirrors and further optimization of the cavity. In addition, diode collimation is critical in side pumped configurations and better collimated diodes are expected to increase the total output power in excess of 30 W levels and should permit 50 W performance levels to be achieved with more attention to cooling. As a final comment, this power range and wide dynamic range is critical to a number of industrial and scientific applications. Single oscillator designs have been developed which have scaled to higher power [17,18], but only operate stably TEM_{00} within a narrow power range that gives the correct thermal lens. Any application that involves changing the repetition rate in Q-switched operation requires a high dynamic range that excludes the use of single power point operation. The above approach gives suitable dynamic range in a practical design for applications ranging from material processing to femtosecond pulse amplification, where the longer storage time of Nd:YLF relative to Nd:YAG offers significant advantages with higher pulse energies.

Acknowledgements

This work was supported by the Natural Sciences and Engineering Research Council of Canada and Photonics Research Ontario.

References

[1] W.L. Nighan Jr., B. Craig, Laser Focus World 32 (1996) 63.
[2] J. Machlan, R. Moyer, D. Hoffmaster, J. Zamel, D. Burchman, R. Tinti, G. Holleman, L. Marabella, H. Injeyan, Technical Digest, ASSL, OSA, 1998, pp. 262–264.
[3] R.J. Shine Jr., A.J. Alfrey, R.L. Byer, Opt. Lett. 20 (1995) 459.
[4] T.S. Rutherford, W.M. Tullock, E.F. Gustafson, R.L. Byer, Technical Digest, CLEO, OSA, 1999, paper CMF6.
[5] M. Karszewski, U. Brauch, K. Contag, A. Giesen, I. Johannsen, C. Stewen, A. Voss, Technical Digest, ASSL, OSA, 1998, pp. 82–84.
[6] J.E. Murray, IEEE J. Quantum Electron. 19 (1983) 488.
[7] H. Vanherzeele, Opt. Lett. 13 (1988) 369.
[8] T.M. Pollak, W.F. Wing, R.J. Grasso, E.P. Chicklis, H.P. Jenssen, IEEE J. Quantum Electron. 18 (1982) 159.
[9] U.S. Patent no. 05048044.
[10] W.A. Clarkson, P.J. Hardman, D.C. Hanna, Opt. Lett. 23 (1998) 1363.
[11] P.J. Hardman, W.A. Clarkson, G.J. Friel, M. Pollnau, D.C. Hanna, IEEE J. Quantum Electron. 35 (1999) 647.
[12] J.M. Eggleston, IEEE J. Quantum Electron. 24 (1988) 1821.
[13] C. Pfistner, R. Weber, H.P. Weber, S. Merazzi, R. Gruber, IEEE J. Quantum Electron. 30 (1994) 1605.
[14] A.K. Cousins, IEEE J. Quantum Electron. 28 (1992) 1057.
[15] M. Tsunekane, N. Taguchi, T. Kasamatsu, H. Inaba, IEEE J. Sel. Top. Quantum Electron. 3 (1997) 9.
[16] http://www.macsh.com/.
[17] W. Schone, S. Knoke, S. Schirmer, A. Tunnermann, Technical Digest, ASSL, OSA, 1997, pp. 241–243.
[18] S. Fujikawa, T. Kojima, K. Yausui, Technical Digest, ASSL, OSA, 1997, pp. 244–246.